Artificial plasma cave in the low-latitude ionosphere results from the radio occultation inversion of the FORMOSAT-3/COSMIC

J. Y. Liu,[1,2] C. Y. Lin,[1] C. H. Lin,[3] H. F. Tsai,[4] S. C. Solomon,[2] Y. Y. Sun,[1] I. T. Lee,[1] W. S. Schreiner,[5] and Y. H. Kuo[5]

[1]   Previous studies report unexpected electron density reductions, termed "plasma caves," located underneath the equatorial ionization anomaly (EIA) crests. A radio occultation (RO) observation simulation experiment has been built to evaluate possible biases introduced by the spherical symmetry assumption in the standard (Abel) RO inversion processes. The experiment simulates the electron density profiles and reconstructs the plasma structure of the EIA at low latitudes, where the horizontal gradient is most significant. The reconstruction shows that artificial plasma caves are created underneath the EIA crests along with three density enhancements in adjacent latitudes. The artifact appears mainly below 250 km altitudes and becomes pronounced when the EIAs are well developed. Above that altitude, the two EIA features in the original (truth) model, the International Reference Ionosphere (IRI-2007), and in the inversion are similar, but the inversion reconstructs less distinct EIA crests with underestimation of the electron density. A simple correction has been introduced by multiplying the ratio between the truth and inversion with actual FORMOSAT-3/COSMIC observations. This initial correction shows that the artificial plasma caves are mitigated. Results also reveal that the RO technique is not suitable to detect or rule out possible existence of the plasma caves.

Citation: Liu, J. Y., C. Y. Lin, C. H. Lin, H. F. Tsai, S. C. Solomon, Y. Y. Sun, I. T. Lee, W. S. Schreiner, and Y. H. Kuo (2010), Artificial plasma cave in the low-latitude ionosphere results from the radio occultation inversion of the FORMOSAT-3/COSMIC, *J. Geophys. Res.*, *115*, A07319, doi:10.1029/2009JA015079.

1. Introduction

[2]   The GPS occultation experiment (GOX) on board the FORMOSAT-3/COSMIC mission, which consists of six microsatellites, has proven to be a powerful tool in probing vertical profiles of the ionospheric electron density by its global-coveraged observations. By accumulating monthly radio occultation (RO) observations, unprecedented detail of the three-dimensional ionospheric electron density structure can be constructed. On the basis of the three-dimensional ionospheric electron density structure of the F3/C GOX observations, details of the equatorial ionization anomaly (EIA) are observed, which is the most pronounced low-latitude ionospheric structure, featured by two dense bands of electron density around ±12°N magnetic latitude

straddling the magnetic equator, discovered 6 decades ago [*Namba and Maeda*, 1939; *Appleton*, 1946; *Duncan*, 1960; *Hanson and Moffett*, 1966; *Anderson*, 1973; *Balan and Bailey*, 1995; *Rishbeth*, 2000]. *Lin et al.* [2007] studies the motions and strength of the EIA crests variations due to the ionospheric seasonal effect. J. Y. Liu and C. H. Lin (Low-latitude ionospheric electron density structure monitored by FORMOSAT-3/COSMIC, paper presented at Second FORMOSAT-3/COSMIC Data Users Workshop, Boulder, Colorado, 2007; Ionospheric plasma cave and depletion bay, paper presented at 5th Annual General Meeting of Asia Oceania Geoscience Society, Busan, Korea, 2008) report for the first time ever observation of unexpected electron density reductions, termed "plasma caves," located underneath the EIA crests. They found that the dimensions of the plasma caves were about 100–150 km in height from the E-peak at about 100 km altitude, about 1100–1650 km in width (10–15°, in latitude), and span around 9900–13200 km in length (90–120°, in longitude; 1200–1800/2000 LT, in local time) and suggested that the EIAs and plasma caves could significantly influence radio propagation and communication.

[3]   Meanwhile, several studies examine the accuracy of the retrieved RO electron density profiles and find that the spherical symmetry assumption required for the Abel inver-

[1]Institute of Space Science, National Central University, Chung-Li, Taiwan.
[2]High Altitude Observatory, National Center for Atmospheric Research, Boulder, Colorado, USA.
[3]Department of Earth Science, National Cheng Kung University, Tainan, Taiwan.
[4]Central Weather Bureau, Taipei, Taiwan.
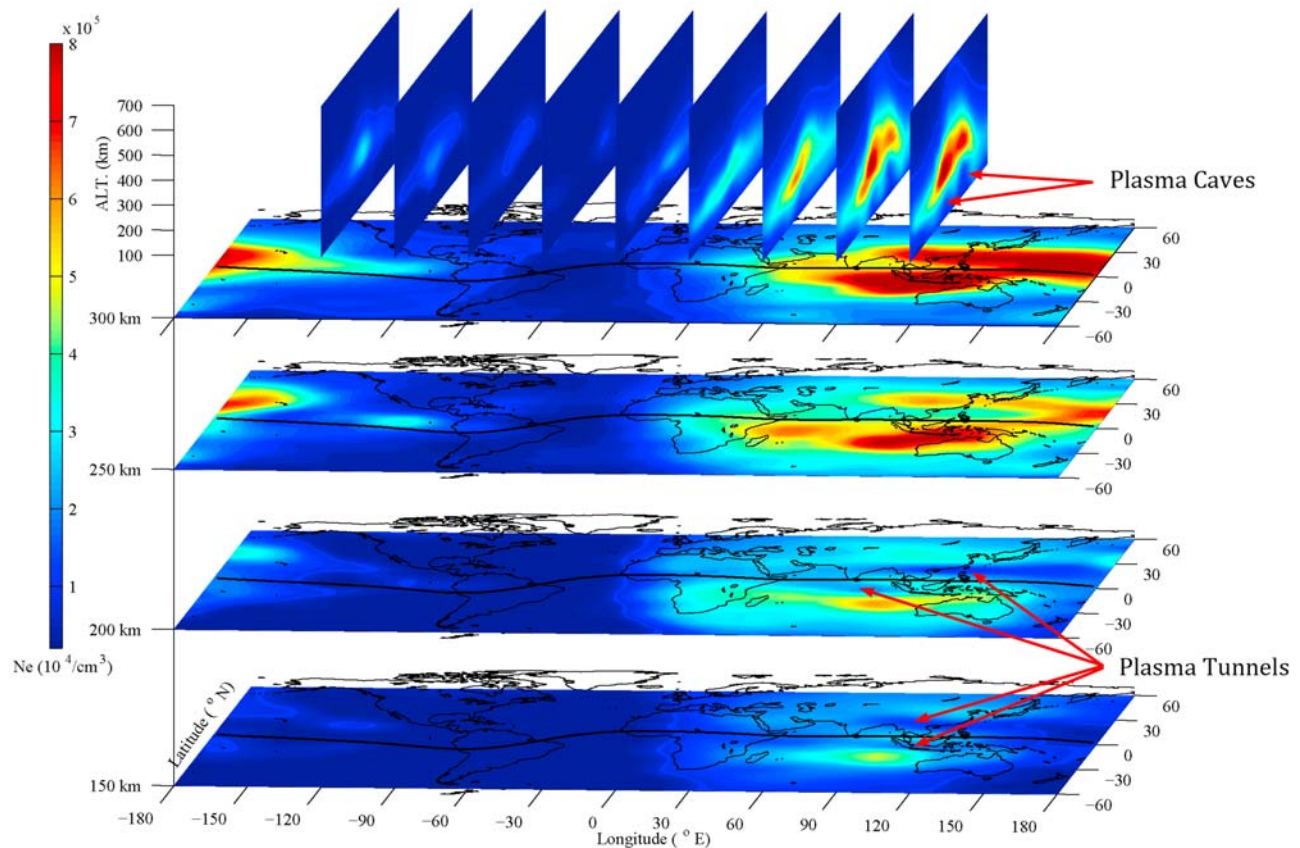[5]COSMIC Project Office, University Corporation for Atmospheric Research, Boulder, Colorado, USA.

Figure 1. Three-dimensional electron density structure observed by the FORMOSAT-3/COSMIC at 0600 UT during April–June 2008. The longitudinal slices in every 30° longitude shown at the top are from −120°E to 120°E geographic longitude. The feature of the plasma caves is shown at below 250 km in 90°E and 120°E longitudes.

sion introduces errors [*Hajj and Romans*, 1998; *Schreiner et al.*, 1999; *Tsai et al.*, 2001; *Tsai and Tsai*, 2004; *Kelley et al.*, 2009; *Liu et al.*, 2010]. *Liu et al.* [2010] further indicate that the spherical symmetry assumption applied around the EIA regions could introduce the significant errors to the bottomside ionosphere around the magnetic equator. In this paper, the international ionosphere reference (IRI-2007) model [cf. *Bilitza and Reinisch*, 2008] and realistic RO locations and raypath geometries of the F3/C observed RO events are used to conduct an observation simulation experiment to assess errors of the electron density caused by the Abel inversion associated with the assumption of spherical symmetry in the EIA regions and to find whether the plasma caves are real. Finally, on the basis of this experiment, a first-order adjustment/correction process is introduced to mitigate the errors.

2. Radio Occultation Observation and Simulation

[4] The F3/C GOX observations are analyzed to reveal the global three-dimensional structure of ionospheric electron density at 0600 UT (universal time) during April–June of 2008 (Figure 1). In these 3 months, the Northern and Southern Hemispheres are in summer and winter seasons, respectively. The most prominent low-latitude ionospheric structure is the EIA crests. It can be seen that during the

daytime period, both vertical and horizontal slices depict two dense bands of electron density at low latitudes straddling the magnetic equator. The dense EIA bands tend to be further away from the magnetic equator at low altitudes and are closer together at higher altitudes in daytime. On the 250 km altitude slice, the south EIA band is closer to the magnetic equator than the north one. Underneath the two EIA crests (side view of the dense bands), two dome-shaped plasma caves are seen in the vertical slices of 90°E and 120°E longitudes. These two caves are also found as depleted bands in the horizontal slices at 150 and 200 km altitudes.

[5] To estimate the error of the RO inversion and to confirm the existence of the plasma caves, the realistic F3/C RO locations and raypath geometries are inserted into the corresponding ionosphere computed by the IRI-2007, to simulate the total electron content (TEC) observed by the GOX. The simulated F3/C GOX TEC is then processed by the standard inversion routine in the COSMIC Data Analysis and Archival Center (CDAAC) to obtain the corresponding electron density profiles. It is worth to note here that the CDAAC ionospheric inversion assumes straight-line propagation of the GPS signal through the ionosphere neglecting the bending angle. The TECs along the raypaths between GPS satellite and F3/C microsatellite are converted to a vertical electron density profile using the Abel transform with an analytical solution to avoid the singularities at the
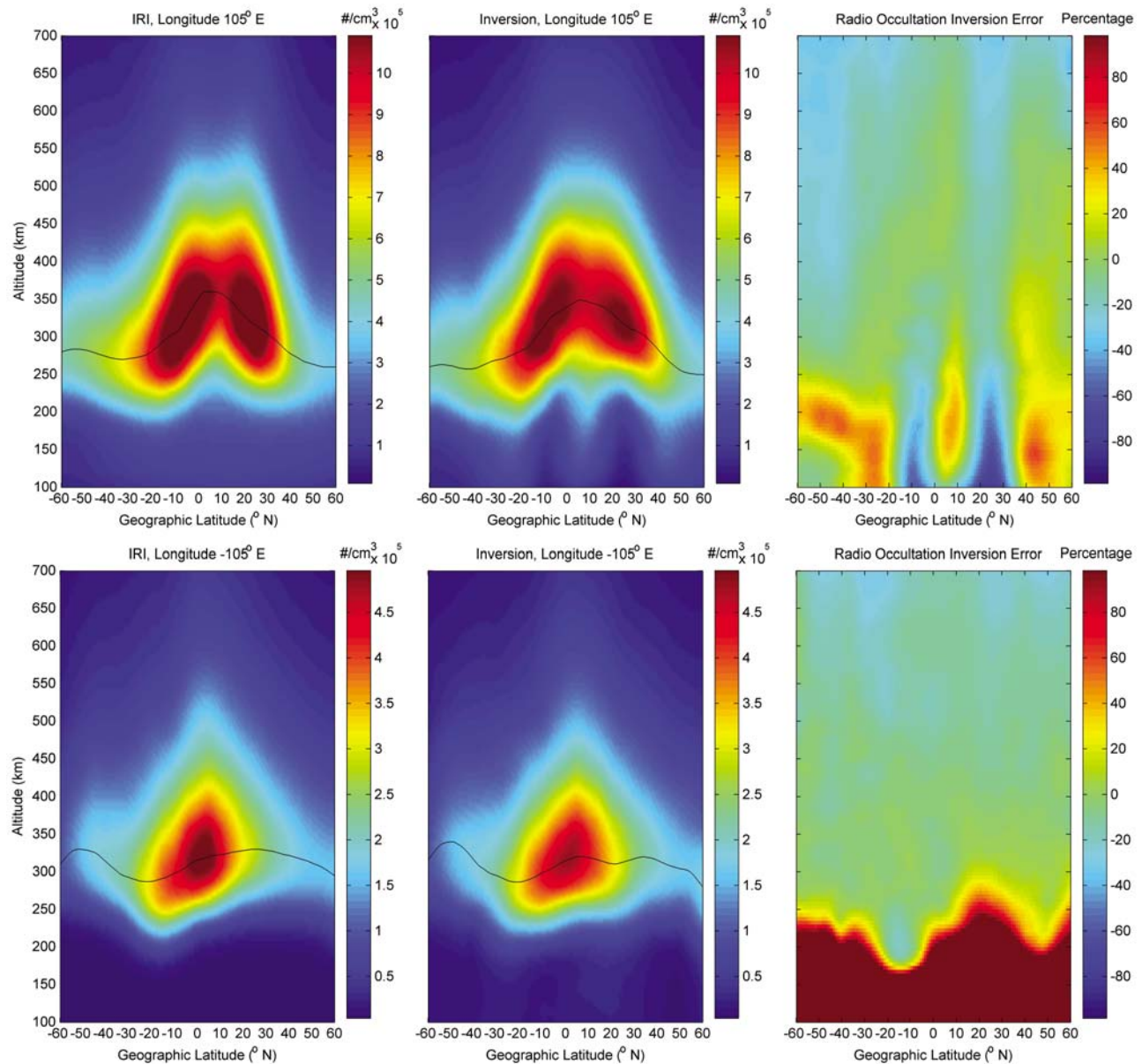
Figure 2. Longitudinal slice of the electron densities of the IRI-2007, the model truth, the RO inversion simulation, and the RO inversion errors at (upper) 105°E (1300 LT) and (lower) −105°E (2300 LT) longitudes at 0600 UT during April–June 2008. Black solid lines represent the hmF_2, and it is noted that Figures 2a and 2b use different colorbar scales in electron densities.

top and lower limits. The major assumptions and approximations used in the CDAAC that may affect the accuracy of the inversion are (1) straight-line GPS signal propagation through the ionosphere, (2) spherical symmetry of the electron densities along the signal raypath, (3) the low Earth orbit satellite F3/C and GPS orbit are close to being coplanar, and (4) first-order estimate of the electron density at the apex altitude for transforming each profile which is made to avoid the integral of Abel inversion to infinity. Among the above items, the major error source comes from the assumption of the spherical symmetry [*Schreiner et al.*, 1999; *Syndergaard et al.*, 2006; *Lei et al.*, 2007]. Here, the ionospheres computed by the IRI-2007 serve as the "truth," and the inverted electron density profiles from simulated

F3/C GOX TEC are the RO inversion simulations. A comparison between the IRI computed ionospheres (IRI_{cmp}) and their RO inversion results (IRI_{ROI}) allows us to estimate the fractional error of the F3/C RO inversion, (IRI_{ROI}-IRI_{cmp})/IRI_{cmp}. The ratio IRI_{cmp}/IRI_{ROI} may be used to mitigate the error of the F3/C actual observations.

[6] Figure 2 displays vertical slices of the IRI_{cmp}, IRI_{ROI}, and error percentage along the 105°E (1300 LT) and −105°E (2300 LT) longitudes. It can be seen that the F3/C inversion weakens the EIA strength and enhances the electron density in the lower ionosphere at magnetic equator and in midlatitudes, which in turn results in the plasma caves appearing under the EIAs at 1300 LT. At 2300 LT longitude sector, the inversion produces a strong over-estimation of the electron
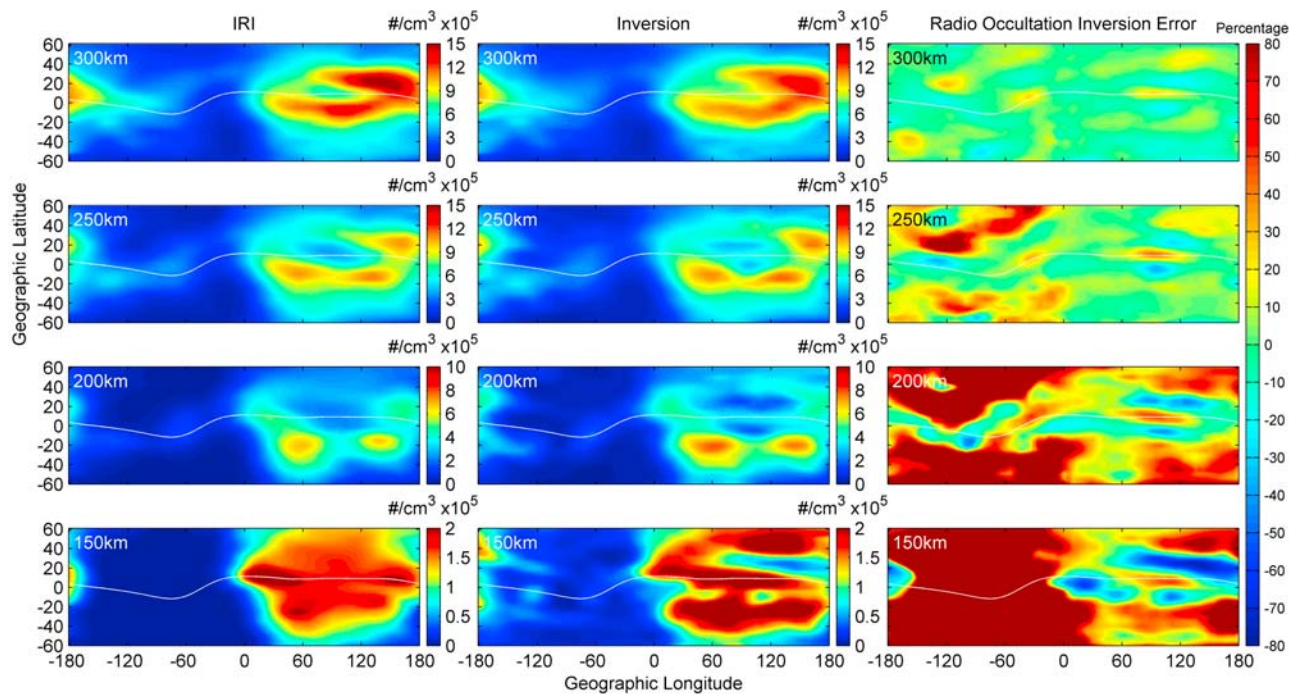
Figure 3. Electron densities at 150, 200, 250, and 300 km altitude obtained from the IRI (the "truth") computation, RO inversion simulation, and RO inversion error at 0600 UT during April–June 2008. It is noted that the color scales vary and the white lines denote the magnetic equator.

densities in lower altitudes. Figure 3 depicts the horizontal slices of the ionospheric electron density of the IRI computation (IRI_{cmp}), associated inversion (IRI_{ROI}), and the error percent at 150, 200, 250, and 300 km altitudes. It can be seen at 150 km altitude that the electron densities at magnetic equator and about 20–30°S yield greater strength from −20° (or 20°W) to 200°E (or 160°W) and 30 to 150°E, respectively. The IRI RO inversion results in two plasma caves (or tunnels) ranging from 60 to 180°E and 30–170°E in the Northern and Southern Hemispheres, respectively, and produces significantly electron density enhancements at magnetic equator between −10 and 175°E. The error percentage further confirms the appearances of the pronounced equatorial enhancement and plasma tunnel reductions simultaneously. Note that the most remarkable cave feature appears at about 20°N, 60–180°E, right under the northern EIA at 300 km altitude. The equatorial enhancement and plasma tunnel features consistently exist but become less prominent from 150 to 250 km altitude in the percentage and have shorter lengths in the longitude direction as altitude increases. Finally, instead of these two features, pronounced dense bands of the EIA features appear at 300 km altitude. Similarities in the F3/C GOX observation result and the IRI observation system simulation experiment indicate that the plasma cave and equatorial enhancement in the lower ionosphere mainly result from the Abel inversion with the assumption of spherical asymmetry applied to the RO data.

3. Error Assessment and Mitigation

[7] Scientists examine concurrent measurements of the ionospheric F2 peak electron density NmF2 and height hmF2 by means of ground-based ionosondes and the Abel inversion of RO observations in the midlatitude and EIA area [*Tsai and Tsai*, 2004] as well as equatorial region [*Liu et al.*, 2010]. *Tsai et al.* [2001] cross-examine the NmF2 (foF2 in the paper) probed by a Digisonde portable sounder (DPS) at Chung-Li (14°N magnetic latitude, the northern EIA area) and colocated GPS/MET soundings from 11 October 1995 to 23 February 1997. They find that the Abel inversion of GPS/MET observations systematically underestimate the electron density near the Chung Li area. On the other hand, *Liu et al.* [2010] compare electron density profiles observed by the F3/C GOX with those obtained by a Digisonde portable sounder, DPS-4, at Jicamarca (12°S, 283°W, 1°N, magnetic) during 2007. They find that at the magnetic equator, the F3/C GOX observations have a tendency to overestimate the daytime electron densities below the F2 peak and underestimate the daytime hmF2. They demonstrate that when a GPS signal transits through EIA crests, it can experience significant increases in the TEC and results in an overestimation of the NmF2 and underestimation of the hmF2 by the F3/C GOX inversions at the magnetic equator [*Liu et al.*, 2010]. These results agree with that the electron density enhancement of the lower ionosphere and the underestimated hmF_2 at magnetic equator obtained by the RO inversion simulation shown in Figure 2. *Tsai et al.* [2001] compared the GPS/MET retrieved ionospheric electron density and ground-based ionosonde data at Chung-Li (the EIA region) and at Bear Lake dynasonde (41.9°N, 111.4°W, midlatitude). They find that the foF2 difference between the GPS/MET retrievals and the colocated ionosonde observations is smaller in the midlatitude at Bear Lake than in the EIA region at Chung-Li. This again indicates that the spherical symmetry
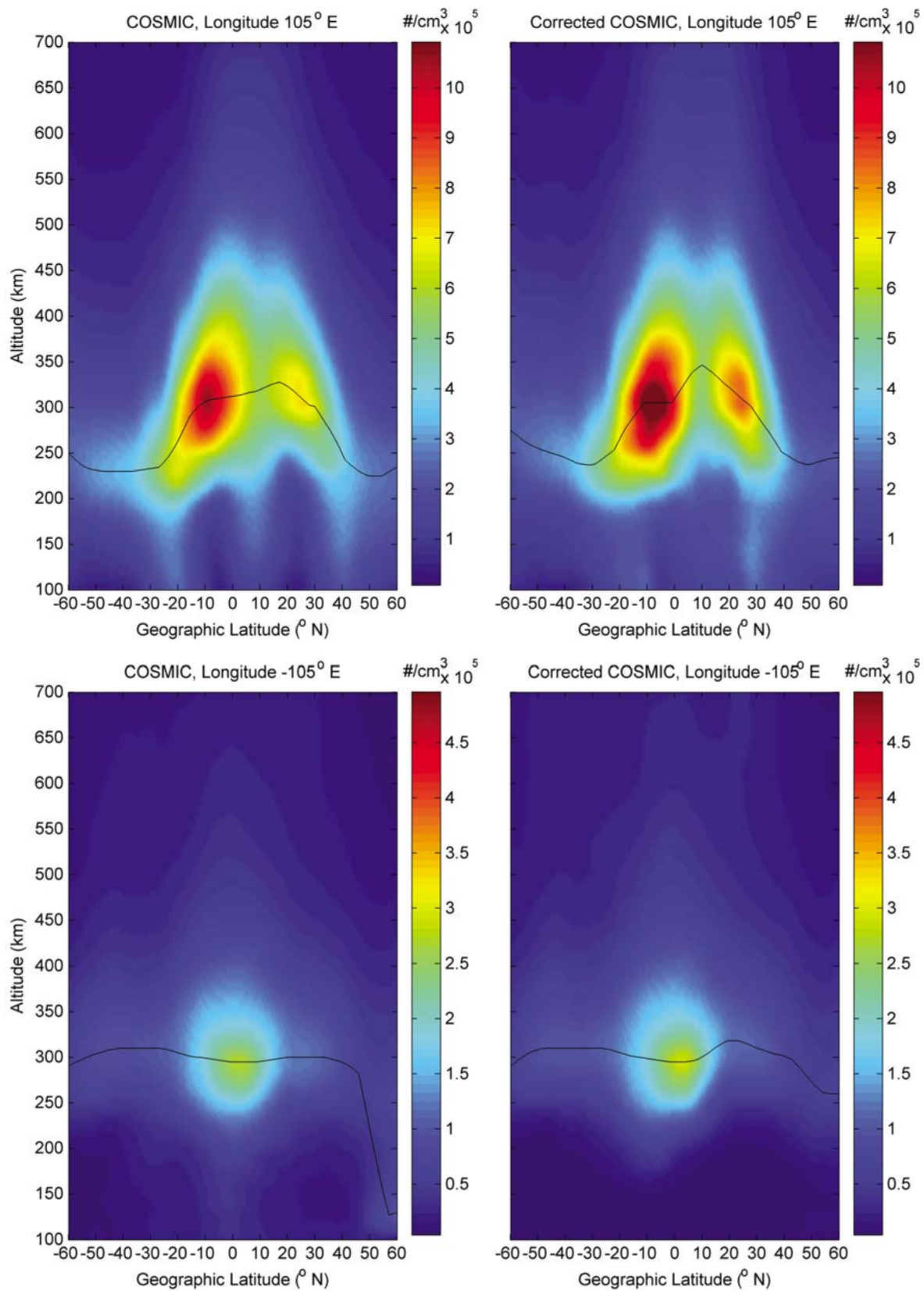
Figure 4. Longitudinal slices of the F3/C electron densities observations and the mitigated electron densities at (upper) 105°E (1300 LT) and (lower) −105°E (2300 LT) longitudes at 0600 UT during April–June 2008. Black solid lines represent the hmF$_2$, and it is noted that Figures 4a and 4b use different colorbar scales in electron densities.
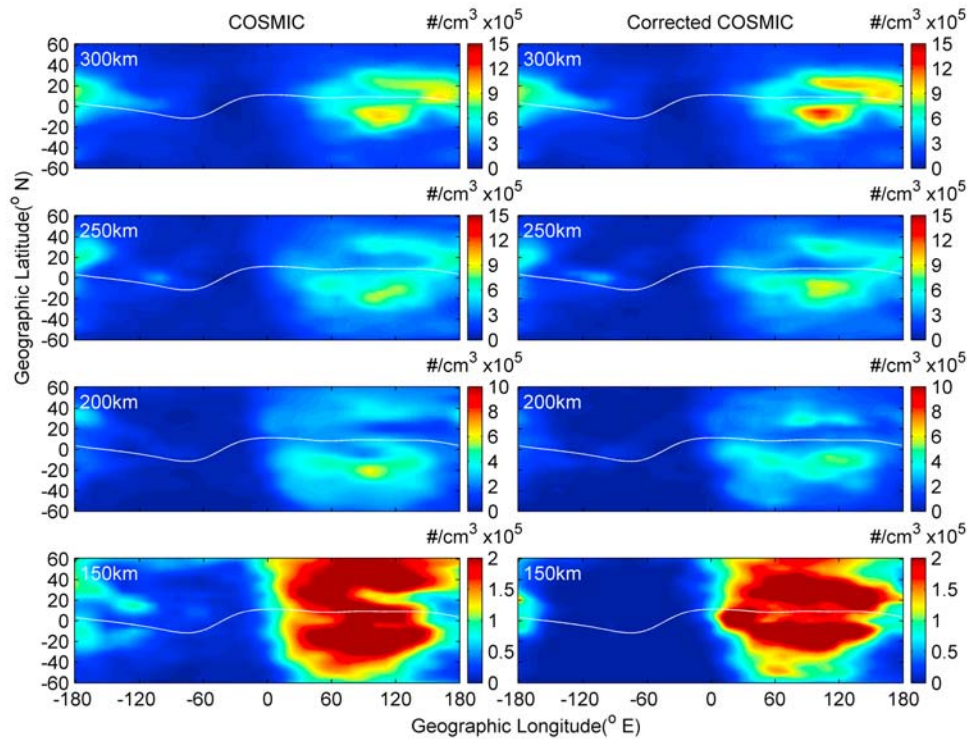
Figure 5. Electron densities at 150, 200, 250, and 300 km altitude obtained from the F3/C observation and the associated mitigated result at 0600 UT during April–June 2008.

assumption required for the Abel inversion introduces significant errors [*Hajj and Romans*, 1998; *Schreiner et al.*, 1999], especially in the EIA area [*Tsai et al.*, 2001; *Tsai and Tsai*, 2004; *Liu et al.*, 2010].

[8] *Kelley et al.* [2009] use the electron density profiles observed by the incoherent scatter radar (ISR) at the Arecibo to validate those inverted from the F3/C colocated observations. They find that the NmF2 probed by the F3/C GOX agrees reasonably with that of the ISR, but the *E* region electron density yields large deviations. They conclude that a simple Abel transform is not suitable for determining the electron density of the lower ionosphere. Our results show that the electron density below the *F* region altitude simulated by the RO inversion indeed largely deviates from the IRI computation, which supports the conclusion reached by *Kelley et al.* [2009].

[9] The previous researches and current study show that the Abel inversion results in significant error in the lower ionosphere by adopting the spherical symmetry assumption but neglecting the horizontal gradient of the ionosphere and the geometric effect. Figure 3 illustrates that the pronounced plasma caves and/or tunnels appear in daytime, and the electron density enhancements systematically occur in the entire nighttime area/period. Note that a RO sounding passing through the two EIA crests enhances the inverted electron densities at the equator and the two poleward sides of the crests (Figure 2, upper). Similarly, for a nighttime sounding, a RO sounding passing through the high electron density area of the *F* region and the low density area of the *E* region results in the electron density in the lower ionosphere constantly being overestimated (Figure 2, lower). In general,

owing to the spherical symmetry assumption, the Abel inversion results in the high electron density regions along the RO sounding path being underestimated and the low ones being overestimated. Here, it is worthwhile to note that due to the nighttime electron density being small, the error percentage in the lower ionosphere becomes much higher in the nighttime period (Figures 2 and 3).

[10] To mitigate the unrealistic plasma caves/tunnels, a first-order approach has been performed as an initial correction, by multiplying the ratios of the computed IRI "truth" and the RO Abel inversion simulation, IRI_{cmp}/IRI_{ROI}, to the F3/C observations after each profile has inverted. Figure 4 displays the slice plots of the F3/C observations and the mitigated and/or corrected results at 105°E (1300 LT) and −105°E (2300 LT) longitudes. It can be seen at 105°E longitude that the plasma cave signatures clearly appear in the F3/C observations before the mitigation is applied, while the mitigated results show obvious improvements in reduction of the plasma caves and enhancement of the EIA crest strength (Figure 4, upper). For nighttime, the significant improvement is seen at −105°E longitude where the lower altitude density enhancements resulted by RO inversion are removed by the simplified correction. The unrealistic low hmF_2 values seen near 50–60°N geographic latitude are corrected as well (Figure 4, lower). Since this is the first-order simplified approach, although reducing the electron density enhancement at the magnetic equator, it still could not fully remove the two electron density enhancements poleward edges of the EIA crests (Figure 4, upper). Horizontal cuts through of the F3/C observations and the mitigated results are shown in Figure 5,

where the artificial three-peaked structure, the plasma tunnels, at 150 and 200 km altitudes are removed. The electron densities at the EIA crests around 300 km altitude are also intensified by the correction.

[11] It should be noted that the simplified correction applied here should be useful if the general electron density structures of the IRI and the F3/C observation are similar. The IRI and F3/C results in both Figures 2 (upper) and 4 (upper) show greater strength and larger altitude extent of the EIA crest in the Southern Hemisphere, while the maximum density lies between the Southern Hemisphere and the equator in Figures 2 (lower) and 4 (lower). Therefore the corrections in this study give relative good improvements in removing the RO inversion errors. On the other hand, if they have large fundamental structural differences, the correction improvement may be limited. Nevertheless, the correction/mitigation performed here simply shows a hint for possible future sophisticated solution of removing the artificial structure resulted from the RO inversion by constructing the comprehensive lookup table or correction function between the EIA and the plasma cave strengths or by developing a detailed data assimilation procedure.

4. Plasma Cave

[12] Liu and Lin (presented paper, 2007, 2008) for the first time report unexpected electron density reductions, with the appearance of plasma caves and tunnels underneath the EIA crests, by means of the F3/C GOX observations. They also find that similar electron density features of the equatorial enhancement and cave reduction the lower ionosphere occasionally appear in an ionosonde chain observation [*Davies*, 1990], IRI computations, TIMED/GUVI limb scans [*Lee et al.*, 2008; J. Y. Liu et al., New features of the ionospheric plasma observed by FORMOSAT-3/COSMIC and other instruments, paper presented at Formosat-3/COSMIC Annual Science Meeting, Taipei, Taiwan, 2008], and in situ electron density measurements at the perigee of the Dynamics Explorer 2 (DE 2) satellite (K. I. Oyama and Y. Kakinami, private communication, 2008). Those measurements show that the caves and/or tunnels become very pronounced in daytime of solar maximum years. To see if the plasma cave/tunnel features can be detected by the F3/C or not in the solar minimum year of 2008, we examine the trough-to-peak ratios of the electron density between the cave trough and the equatorial enhancement for both the RO inversion simulation and the F3/C observation. A detailed study shows that at 150 (200) km altitude along the longitude 105°E, the ratios in the RO simulations are 0.73 (0.58) and 0.6 (0.55) in the Northern and Southern Hemispheres, respectively, while those of the F3/C observations are 0.63 (0.58) and 0.66 (0.50), respectively. Since the peak-to-trough ratios of the simulated result and the real F3/C observation are in compatible magnitudes, we cannot detect or rule out possible plasma caves by means of the F3/C GOX observations.

5. Summary and Conclusion

[13] The observation simulation experiment carried out in this study shows that the RO sounding can obtain reasonably correct electron density around and above the F2 peak, and however, the assumption of spherical symmetry introduces artificial plasma cave and plasma tunnel structures as well as the electron density enhancement at the magnetic equator at and below 250 km altitude during daytime. A first-order correction has been performed to mitigate the artifact. The initial result shows that the artificial plasma cave (tunnel) and especially the enhancement features could be partially mitigated. This positive result of the mitigation/correction provides hints for future sophisticated solution of the artifact. Meanwhile, the peak-to-trough ratios of the simulated result and the real F3/C observation have compatible magnitudes, which indicate that the RO technique is not suitable to study the plasma caves. In conclusion, the ionospheric electron densities derived by the RO sounding around and above the F2 peak yield reasonably correct, and however, those below the *F* region should be extremely carefully used.

References

Anderson, D. N. (1973), A theoretical study of the ionospheric *F* region equatorial anomaly, I, Theory, *Planet. Space Sci.*, *21*, 409–419, doi:10.1016/0032-0633(73)90040-8.

Appleton, E. V. (1946), Two anomalies in the ionosphere, *Nature*, *157*, 691, doi:10.1038/157691a0.

Balan, N., and G. J. Bailey (1995), Equatorial plasma fountain and its effects: Possibility of an additional layer, *J. Geophys. Res.*, *100*(A11), 21,421–21,432, doi:10.1029/95JA01555.

Bilitza, D., and B. Reinisch (2008), International Reference Ionosphere 2007: Improvements and new parameters, *Adv. Space Res.*, *42*(4), 599–609, doi:10.1016/j.asr.2007.07.048.

Davies, K. (1990), *Ionospheric Radio*, Peter Peregrinus, London.

Duncan, R. A. (1960), The equatorial *F* region of the ionosphere, *J. Atmos. Terr. Phys.*, *18*, 89–100, doi:10.1016/0021-9169(60)90081-7.

Hajj, G. A., and L. J. Romans (1998), Ionospheric electron density profiles obtained with the global positioning system: Results from the GPS/MET experiment, *Radio Sci.*, *33*, 175–190, doi:10.1029/97RS03183.

Hanson, W. B., and R. J. Moffett (1966), Ionization transport effects in the equatorial *F* region, *J. Geophys. Res.*, *71*, 5559–5572.

Kelley, M. C., V. K. Wong, N. Aponte, C. Coker, A. J. Mannucci, and A. Komjathy (2009), Comparison of COSMIC occultation-based electron density profiles and TIP observations with Arecibo incoherent scatter radar data, *Radio Sci.*, *44*, RS4011, doi:10.1029/2008RS004087.

Lee, I. T., J. Y. Liu, P. K. Rajesh, and C. H. Lin (2008), The structure of equatorial ionization anomaly seen by TIMED/GUVI limb observations, *Eos Trans. AGU*, *89*(53), Fall Meet. Suppl., Abstract SA21A-1527.

Lei, J., et al. (2007), Comparison of COSMIC ionospheric measurements with ground-based observations and model predictions: Preliminary results, *J. Geophys. Res.*, *112*, A07308, doi:10.1029/2006JA012240.

Lin, C. H., J. Y. Liu, T. W. Fang, P. Y. Chang, H. F. Tsai, C. H. Chen, and C. C. Hsiao (2007), Motions of the equatorial ionization anomaly crests imaged by FORMOSAT-3/COSMIC, *Geophys. Res. Lett.*, *34*, L19101, doi:10.1029/2007GL030741.

Liu, J. Y., C. C. Lee, J. Y. Yang, C. C. Chen, and B. W. Reinisch (2010), Electron density profiles in the equatorial ionosphere observed by the FORMOSAT-3/COSMIC and a Digisonde at Jicamarca, *GPS Solut.*, *14*, 75–81, doi:10.1007/s10291-009-0150-3.

Namba, S., and K.-I. Maeda (1939), *Radio Wave Propagation*, 86 pp., Corona, Tokyo.

Rishbeth, H. (2000), The equatorial F-layer: Progress and puzzles, *Ann. Geophys.*, *18*, 730–739, doi:10.1007/s00585-000-0730-6.

Schreiner, W. S., S. V. Sokolovsky, and C. Rocken (1999), Analysis and validation of GPS/MET radio occultation data in the ionosphere, *Radio Sci.*, *34*, 949–966, doi:10.1029/1999RS900034.

Syndergaard, S., W. S. Schreiner, C. Rocken, D. C. Hunt, and K. F. Dymond (2006), Preparing for COSMIC: Inversion and analysis of ionospheric data products, in *Atmosphere and Climate: Studies by Occultation Methods*, edited by U. Foelsche, G. Kirchengast, and A. K. Steiner, pp. 137–146, Springer, Berlin.

Tsai, L. C., and W. H. Tsai (2004), Improvement of GPS/MET ionospheric profiling and validation using the Chung-Li ionosonde measurements and the IRI model, *Terr. Atmos. Ocean. Sci*, *15*, 589–607.

Tsai, L. C., W. H. Tsai, W. S. Schreiner, F. T. Berkey, and J. Y. Liu (2001), Comparisons of GPS/MET retrieved ionospheric electron density and ground based ionosonde data, *Earth Planets Space*, *53*, 193–205.

Y. H. Kuo and W. S. Schreiner, COSMIC Project Office, University Corporation for Atmospheric Research, Boulder, CO 80305, USA.

I. T. Lee, C. Y. Lin, J. Y. Liu, and Y. Y. Sun, Institute of Space Science, National Central University, Chung-Li 32001, Taiwan. (jyliu@jupiter.ss.ncu.edu.tw)

C. H. Lin, Department of Earth Science, National Cheng Kung University, Tainan 701, Taiwan.

S. C. Solomon, High Altitude Observatory, National Center for Atmospheric Research, Boulder, CO 80305, USA.

H. F. Tsai, Central Weather Bureau, Taipei 10048, Taiwan.